Journal of Computer-Aided Molecular Design **17:** 551–565, 2003.

Modeling of enzyme–substrate complexes for the metalloproteases MMP-3, ADAM-9 and ADAM-10

Sergio Manzetti[a,b,c,d], Daniel R. McCulloch[a], Adrian C. Herington[a] & David van der Spoel[e,*]
[a]*Centre for Molecular Biotechnology, School of Life Sciences, GPO Box 2434, Queensland University of Technology, Brisbane, Queensland 4001, Australia;* [b]*Proinformatix.com, Øvre Lippestad Gaard, 1825 Tomter, Norway;* [c]*Biozentrum, University of Basel, Klingelbergstr. 70, CH-4056 Basel, Switzerland;* [d]*Institute of Cellular and Molecular Biology, Biology Department, University of Oslo, Blindernveien, 0371 Oslo, Norway;* [e]*Biomedical Center, Department of Cell and Molecular Biology, Husargatan 3, Box 596, S-75124 Uppsala, Sweden*

Received 1 November 2002; accepted 24 July 2003

Key words: ADAM (A Disintegrin And Metalloprotease domain), cancer, catalytic mechanism, GROMACS, matrix metalloproteases (MMPs), substrate specificity

Summary

The matrix metalloproteases (MMPs) and the ADAMs (A Disintegrin And Metalloprotease domain) are proteolytic enzyme families containing a catalytic zinc ion, that are implicated in a variety of normal and pathological processes involving tissue remodeling and cancer. Synthetic MMP inhibitors have been designed for applications in pathological situations. However, a greater understanding of substrate binding and the catalytic mechanism is required so that more effective and selective inhibitors may be developed for both experimental and clinical purposes. By modeling a natural substrate spanning P4-P4′ in complex with the catalytic domains, we aim to compare substrate-specificities between Stromelysin-1 (MMP-3), ADAM-9 and ADAM–10, with the aid of molecular dynamics simulations. Our results show that the substrate retains a favourable antiparallel beta-sheet conformation on the P-side in addition to the well-known orientation of the P′-region of the scissile bond, and that the primary substrate selectivity is dominated by the sidechains in the S1′ pocket and the S2/S3 region. ADAM-9 has a hydrophobic residue as the central determinant in the S1′ pocket, while ADAM-10 has an amphiphilic residue, which suggests a different primary specificity. The S2/S3 pocket is largely hydrophobic in all three enzymes. Inspired by our molecular dynamics calculations and supported by a large body of literature, we propose a novel, hypothetical, catalytic mechanism where the Zn-ion polarizes the oxygens from the catalytic glutamate to form a nucleophile, leading to a tetrahedral oxyanion anhydride transition state.

Introduction

The matrix metalloproteases (MMPs) and the ADAMs (A Disintegrin And Metalloprotease domain) are members of the metzincin (zinc dependent metalloprotease) superfamily [1–3]. Many of these enzymes have the ability to cleave, activate and solubilize growth factors such as tumor necrosis factor α (TNF α), transforming growth factor β (TGF β), heparin-binding epidermal growth factor (HB-EGF) and interleukins, as well as components of the basement membrane (BM) and extracellular matrix (ECM), including collagen type IV and fibronectin [4–8]. Both families are involved in normal as well as pathological processes including embryonic development, cell growth and proliferation, inflammatory responses, wound repair, multiple sclerosis, arthritis and cancer progression and metastasis [1–3]. To date, 20 distinct MMPs and 33 ADAMs have been described, although not all ADAMs are catalytically active proteases. The presence of a disintegrin domain in the ADAMs proteins, which has been shown to bind to integrins on cell surfaces, further highlights the possibility that the ADAM

*To whom correspondence should be addressed. E-mail: spoel@xray.bmc.uu.se

proteases are involved in regulation of cell–cell or cell–ECM contacts, as well as in ECM degradation. Both these functions are critical for regulating cell migration and invasion – two key stages in the complex process of cancer cell metastasis.

Both MMPs and ADAMs are synthesized as zymogens, and activated by a cysteine switch mechanism [9]. They share a homologous catalytic motif (consensus HEXXHXXGXXHX) in their N-terminally-located metalloprotease domain. This motif contains a His-triad responsible for the stabilisation of a catalytic Zn-ion [10], and a conserved catalytic glutamate [11]. Previous studies by Browner et al. [12] suggest the catalytic mechanism of zinc metalloproteases to be a general base-catalysis, carried out by the Zn-ion, a glutamate and a putative water molecule. A second, non-catalytic Zn-ion, which is found in the MMPs, is thought to be structurally important but not catalytically active [13–15].

Under normal circumstances, metalloprotease action is regulated by naturally-occurring inhibitors. For MMPs these inhibitors are the tissue inhibitors of the MMPs (TIMPs), which bind to MMPs in a 1:1 stoichiometry [16]. Recently, it has been demonstrated that some of the ADAMs proteases, specifically ADAM-10 and -17, are also inhibited by TIMPs [17, 18]. Based primarily on crystal structures of MMPs with substrate analogues and partly on the knowledge of their mechanisms of action, a variety of effective synthetic inhibitors have been developed and a number of these have been assessed in clinical trials, for subsequent use as therapeutic agents [19], albeit with limited success. Insufficient information is available on the structures, substrate specificity, dynamics and catalytic mechanisms, particularly for the ADAMs, to allow further developments in understanding of the potential diagnostic or therapeutic utilization of these enzymes. A major aim of this work is to address these issues for ADAM-9 and -10 in particular. ADAM-9 and -10 were chosen because they share significant substrate specificity, structural and activation characteristics with MMPs. Like several MMPs, bovine ADAM-10 has been shown to cleave wild type collagen type IV [20] *in vitro* and it seems likely that human ADAM-10 will degrade the same substrate. ADAM-9 recombinant metalloprotease domain has recently been shown to cleave fibronectin, gelatins and the insulin B-chain, again demonstrating substrate overlap with the MMPs [8].

In this study we used the crystal structure of MMP-3 in complex with TIMP-1 [21] to construct an enzyme-substrate model spanning P4-P4′ for MMP-3. Using homology modeling in combination with molecular dynamics refinement in explicit solvent, we build models of ADAM-9 and ADAM-10 enzyme/substrate complexes. With this approach we are able to describe subsites and interactions in the binding regions that are useful in understanding the binding mechanism. Our results provide new information about structure and substrate binding similarities between members of the MMPs and ADAMs. This is important for identifying candidate metzincins in terms of their involvement in the pathogenesis of particular physiological/disease processes and for the further development of alternative and perhaps more effective metalloprotease inhibitors, not only broad spectrum compounds but also inhibitors specific for individual MMPs or ADAMs. Additionally, this study provides support for a novel (zinc-mediated) catalytic mechanism, emphasizing the need to further our understanding of the mechanism of metzincin-substrate binding and catalysis.

Materials and methods

Protein modeling

MMP-3 in complex with a hypothetical substrate

All homology modeling approaches were performed using the SWISS Model suite [20]. The structure of the MMP-3/TIMP-1 complex [21] (PDBid: 1UEA) was retrieved from the PDB (protein databank [22]). After a structural superimposition, the enzyme was replaced with the equivalent structure crystallized by Chen et al. [23] (PDBid: 1B3D). This was done so that the conformational change in the enzyme at the substrate binding cleft [23] could be accounted for in our simulations, since the N-terminal region of TIMP-1 approaches the S-region of the enzyme. All residues from TIMP-1 except for the P′-mimicking N-terminal residues were then intentionally removed. All details of binding between the N-terminal segment of TIMP-1 and the MMP-3 structure were successfully reproduced, with retention of the native H-bond coordination.

The substrate was modeled by preserving the P′-region from TIMP-1 and adding five residues to its cysteine residue at P1′ [24]. The P-segment was modeled by adjusting its ϕ/ψ angles in an antiparallel β-sheet conformation H-bonded to the adjacent substrate binding β-sheet from the enzyme (Figure 1).

The substrate for MMP-3 consisted therefore of the following sequence: GPLA↓TCVP (where the GPLA motif at the P-region was taken from Smith et al. [24], and the remaining residues are from TIMP-1).

The catalytic domains of ADAM-9 and ADAM-10. The sequences of ADAM-9 and ADAM-10 were retrieved from the Entrez database (http://www.ncbi.nih.gov/Entrez), access nos. NP_003807 and NP_001101, respectively. For the homology modeling the sequences of the catalytic domains for ADAM-9 (L208-I405 [25]), and for ADAM-10 (E217-V452) were modeled using the optimal approach mode in the SWISS Model suite [20], with an enhancement of the structural alignment using the SAM-T99 alignment tune-up interface [26] at http://www.cse.ucsc.edu/research/compbio/HMM-apps, followed by a manual threading optimisation. ADAM-9 was modelled in two steps: first, 1QUAa was used as template for correct disulphide and substrate-binding β-sheet modeling and second, 3AIG was used to construct another model with a correctly modelled Met-turn. The correctly modelled Met-turn, where the methionine sidechain is directed inwards, behind the Zn-ion, replaced the equivalent segment of the first model, where the sidechain of the methionine was oriented outwards. In this manner, the final candidate for ADAM-9 contained correct disulphide coordination, the substrate-binding beta-sheet and a plausible Met-turn. Due to a smaller number of suitable templates for ADAM-10 only the structure of TACE (ADAM-17, 1BKCi [27]) was used for the homology modeling. All regions were modeled with homologous regions in the template, except for the reprolysin-loop. The catalytic Zn-ion was added to ADAM-9 and -10 by superimposing each model with the crystal structure of atrolysin-C (PDBid 1HTDb [28]).

ADAM-9 and ADAM-10 in complex with their hypothetical substrates. ADAM-9 and ADAM-10 were separately superimposed with the pre-refined MMP-3–substrate complex (see next paragraph). The substrate from the MMP-3–substrate complex was then copied to the structures of ADAM-9 and ADAM-10, respectively. Using a database of rotamer values (included with the SWISS Model suite), the residues on the substrate chain were mutated to insert the following residues in the substrate. For ADAM-9 the substrate was AALY↓LVCG (Insulin B-chain [8]) where the alanine at P4 was derived from other well-hydrolysed peptides from the same study [8] (this combination was applied because negatively charged residues at the P4-position affected Zn-coordination at the catalytic center during preliminary simulations). The substrate for ADAM-10 was LAGA↓VMSS (Pro-TNF [7]), where the methionine at the P2′-position was chosen based on the results of Vincent et al. [5]. An arginine at this position (as found in Pro-TNF) disturbed the catalytic centre by forming a salt-bridge with the catalytic glutamate in preliminary molecular dynamics simulations. The Gln at the P2 positions was replaced by a glycine because of steric problems. Because of the structural differences between the two ADAMs and MMP-3, a manual adjustment of the substrate was performed to approach the H-bonding pattern at the P′-region found in metzincins [29]. Changes in the ϕ/ψ angles of the P-segment were applied to the β-sheet area on the Ramachandran plot to extend the H-bonding antiparallel with the substrate binding β-sheets (Figure 2).

Structure refinement and molecular simulation

All complexes were subjected to a steepest descent energy minimization of 500 steps, with the GROMOS96 43b1 vacuum force field [30]. MMP-3 was minimized only at the residues from the P-side of the substrate and its neighbors within 0.6 nm from the enzyme, because the starting structure was derived from a crystal structure. Subsequently, MMP-3, ADAM-9 and ADAM-10, in complex with their respective substrates, were confined in rectangular boxes filled with roughly 7600, 6000 and 9000 water molecules respectively, and counterions (Na^+ and Cl^-) to neutralize the system. The solvated complexes were then energy-minimized through 100 steps prior to molecular dynamics (MD) simulations. After this the complexes were submitted to 100 ps restrained MD where the non-hydrogen atoms of the proteins were restrained to their starting positions with a force constant of 1000 kJ/mol nm^{-2}. For ADAM-9 and ADAM-10 two independent simulations were performed with different starting velocities, in order to generate different trajectories, and hence test the stability of the models. For MMP-3 a single simulation was done, since this system is based on a crystal structure rather than a homology model. The production MD simulations were carried out at 300 K for 2 ns with a time-step of 2 fs using the GROMOS96 43a1 force field [30] and the simple point charge water model [31]. The GROMACS 3.1 simulation package was

used for all simulation and trajectory analysis [32]. The bonds in the protein were constrained using the LINCS algorithm [33] whereas the water molecules were constrained using the SETTLE algorithm [34]. All N- and C-termini were assigned a neutral state, because they are not natural termini, and therefore introducing full charges might lead to artefacts. Furthermore, since the description of ions in proteins in a classical model is problematic due to polarization and charge transfer effects, we applied distance restraints to maintain the Zn- and Ca-ions in the correct ligation state [35]. The distance restraints were modeled such that whenever the distance between ion and ligand (for the catalytic Zn the Nε of the two histidines only) was more than 0.1 nm beyond the starting model (the crystal structure in the case of MMP3) a force was applied, proportional to the distance beyond 0.1 nm with a force constant of 1000 kJ/mol nm^2. This implies that the forces in the starting conformation are zero, and generally that the disturbance of the starting model (crystal structure) is minimal. Other approaches to model ion ligation in molecular simulation have been to use stronger forces [36], or even covalent bonds, which is not a correct treatment for the ions in our models either. Finally, the nominal charge of $+2$ was used for Zn and Ca ions, as it is not possible within the approximations of classical molecular simulation to model charge transfer correctly. The choice of calcium-chelating atoms in the distance restraints was derived from experimental data of the crystal structures of MMP-3 [23]. The Zn-chelating histidine residues were protonated at the δ-nitrogen, as observed in crystal structures of MMPs [23]. Energies and coordinates were saved once per picosecond and temperature and pressure coupling were carried out using the Berendsen scheme [37]. Long-range electrostatics were simulated using the particle-mesh Ewald method [38], whereas a Van der Waals cut-off of 1 nm was used (although the GROMOS96 force field was developed with a twin-range cut-off of 0.8/1.4 nm). Neighborlists were used and updated every 10 fs.

Enzyme/substrate interfaces

The enzyme/substrate contacts were monitored over the last 1000 ps of the simulations using the program g_mdmat, part of the GROMACS 3.1 package [32]. The interactions resulting from the contact map analyses were inspected visually with SWISS PDB Viewer [20].

Results and discussion

Protein modeling

Modeling of ADAM-9 and ADAM-10 showed that the catalytic domains of these enzymes are most similar to the snake venom metalloprotease Atrolysin-C (rmsd 0.22 nm) and TNF-alpha Converting Enzyme (ADAM-17) (rmsd 0.3 nm), respectively. The available structural data of Adamalysin II [39], Atrolysin-C [28], Acutolysin-C [40], and TACE [27] from the Protein Databank give insight into the coordination of disulphide bridges in ADAM-9 and ADAM-10. ADAM-9 has the same coordination of disulphide bridges as found in its primary template Acutolysin-C (32.6% identity). Cys322-Cys401 anchors the long loop (Phe317-Ala327) that follows the anti-parallel substrate-binding β-sheet, with the N-terminal region (Table 1). Cys363-Cys385 and Cys365-Cys370 stabilize a 15-residue segment between the third histidine from the Zn-chelating triad and the Met-turn, and hence it seems that these disulphides are important for the structural stability in this region.

The structure of ADAM-17 [27] was the only template for the modeling of ADAM-10 (30% identity). Like its template, ADAM-10 has three disulphide bridges. The first, Cys221-Cys312, connects the second and the third antiparallel β-strands of the five β-strands that are typically found in metalloproteases. This disulphide bond is not found in either adamalysins or matrixins, and is a signature of reprolysins. The second, Cys343-Cys450, connects the C-terminus with the loop that follows the substrate-binding β-strand as in adamalysins (Table 1). The third, Cys398-Cys434, connects the start of the C-terminal helix with the turn that precedes the Met-turn, and is a disulphide bond also found in adamalysins. We think that the carefully modelled Met-turns, secondary structure prediction of the substrate-binding beta sheets of ADAM-9 and ADAM-10 (data not shown), and the well-defined catalytic center containing the Zn-binding site provides a strong basis for use of our models in assessment of substrate preference.

Enzyme-substrate building

The modeling of the enzyme–substrate complex for MMP-3 was based on the natural MMP-3/TIMP-1 complex [21] and the synthetic MMP-3/hydroxamate inhibitor complex [23]. Preliminary binding pocket analysis with VIDA (Openeye Scientific Software, Santa Fe, USA) shows that the binding pocket runs

Table 1. Residues from the β-sheets involved in substrate binding via H-bonds, listed before and after molecular simulation. Residues marked with an asterisk indicate the corresponding residues from the reference simulation of MMP-3 crystallized by Gomis-Rüth et al. [21]. The residues marked with * indicate the H-bonding residues interacting with the substrate. Sim. 1, first simulation; Sim. 2, second simulation.

ADAM-9	Before MD	After 2 ns MD
Substrate-binding beta-sheet	Gly311-Ala316	Sim. 1: Gly311-Val318
		Sim. 2: Gly314-Ala316
Substrate-binding beta anchor	Ser374*	Sim. 1: Asn373*
		Sim. 2: –
ADAM-10	Before 2 ns	After 2 ns
Substrate-binding beta-sheet	Gly325-Trp331	Sim. 1: Gly325-Trp331
		Sim. 2: Leu327-Trp331
Substrate-binding beta anchor	Ala421*	Sim. 1: Ala418-Ala420
		Sim. 2: Ala418-Ala420
MMP-3	Before 2 ns	After 2 ns
Substrate-binding beta-sheet	Asn162-Ala169*	Asn162-Ala169
Substrate-binding beta anchor	Pro221-Tyr223*	Pro221-Tyr223

Table 2. Subsites for MMP-3, ADAM-9 and ADAM-10. The table lists the residues from the enzyme that are involved in interaction with the substrate, during the 2 ns-simulation. Common residues that occurred twice are considered as subsites. The residues marked with an asterisk indicate the interactions that were computed based on the crystallized P′-region of MMP-3/TIMP-1 [21].

MMP-3	S4	S3	S2	S1	*S1′	*S2′	*S3′	*S4′
	Phe210	Phe210	Ala167	Solv	Leu164	Solv	Solv	Solv
	Phe83	Ala169	Ser206	His166	Val198	Val163	Leu164	Leu222
				His211	Pro221			
ADAM9	S4	S3	S2	S1	S1′	S2′	S3′	S4′
Sim. 1	Phe317	Val318	Val318	Met315	Ile344,	Solv	Solv	Solv
	Val318	Met315	His351	Solv	Ala313	Asn373	Ser374	Gly310
			Asn356		Asn373	Thr312		
Sim. 2	His357	Tyr-P1	Val318	Met315	Ile344	Solv	Solv	Solv
	Solv	Met315	His351	Solv	Asn373	Asn373	Ser374	
				His357	Solv	Thr312	Phe333	
ADAM10	S4	S3	S2	S1	S1′	S2′	S3′	S4′
Sim. 1	Pro391	Val332	Val332	Leu329	Leu327	Solv	Solv	Solv
	Val332	Pro391	Solv	Solv	Thr379	Val326	Asn366	Thr421
					Ala418			
Sim. 2	Val332	Val332	Solv	Leu329	Leu327	Solv	Solv	Solv
	Trp331	Asn387	His392	His392	Thr379	Val326	Asn366	Arg421
				Solv	Ala418			

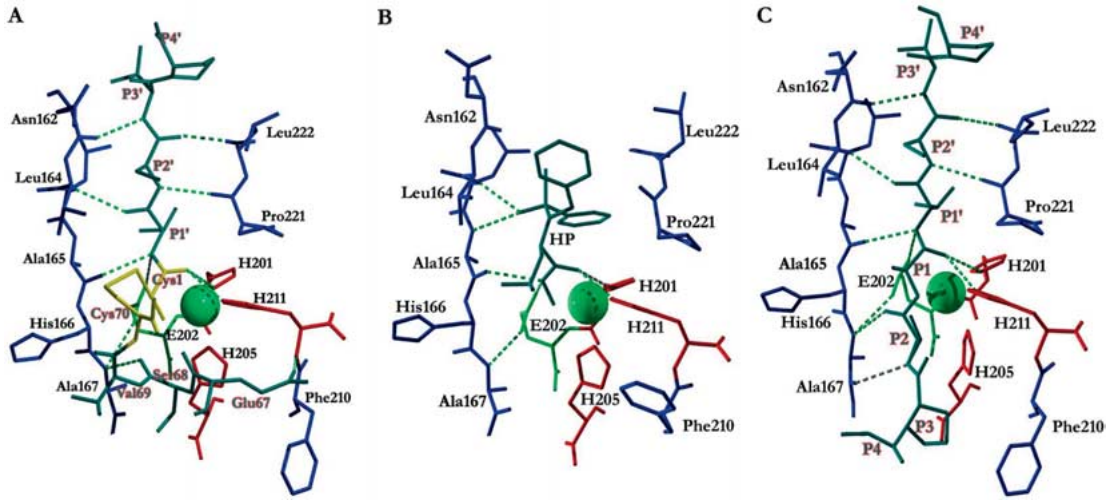

Figure 1. The enzyme–substrate complex for MMP-3 with three different ligands. The enzyme is coloured in blue, the catalytic glutamate, E202 and the Zn-ion are coloured in light green, as are the H-bonds, while the Zn-ligands, H201, H205 and H211, are coloured in red. (A) Binding pocket and intramolecular H-bonds between the enzyme and the P′- and P-segments from TIMP-1 interconnected with a disulphide bridge between Cys1-Cys70 (yellow, noted with P1′, P2′, . . . on the P′-side and Cys70, Val69, Ser68 on the P-side [21]); (B) binding pocket of MMP-3 with hydroxamate phosphinamide inhibitor (HP, dark green) with intramolecular H-bonds [23]; (C) the MMP-3 enzyme–substrate complex modelled on the basis of the two former complexes, the scissile bond is located between P1′ and P1, residues from P3′-P3 are extended in a beta-sheet conformation (this work).

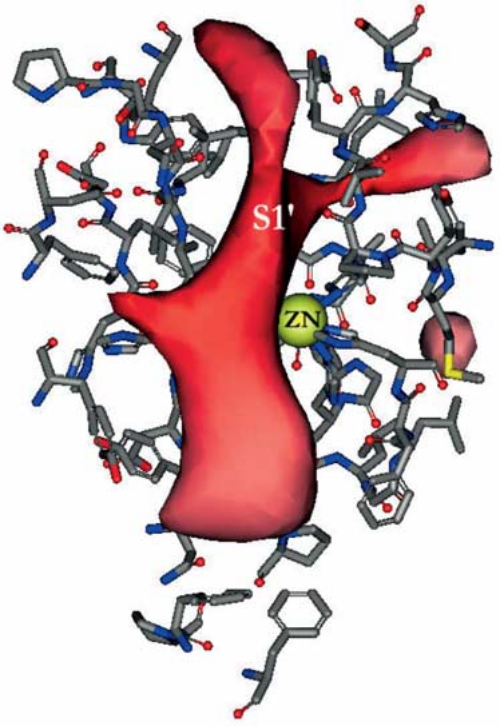

Figure 2. The substrate-binding pocket of MMP-3. The surface generated with FRED (Openeye Scientific Software, Santa Fe, USA) shows that there is a large binding space below the Zn-ion (yellow), which designates the P-region. This is useful to determine how the substrate can orient itself from the P′-region.

from the P′-region downwards, past the catalytic center, into the P-region (Figure 2), which contributes to the hydrophobic binding of TIMP-1 inhibitor [21]. However, the exact position of the scissile bond and the torsions of the residues from P1′ to the P-region are not known. In order to find a natural orientation, a comparison between the synthetic and natural inhibitor complex structures was carried out. This comparison (Figure 1) shows that the catalytic center is virtually identical in the natural and synthetic inhibition situation, and that the P′-region is stabilized by the same residues through backbone H-bonds in both a synthetic and natural inhibition. This accommodation, combined with the position of the N-terminal nitrogen from TIMP-1 [21], suggests that the scissile bond (Figure 1) is located slightly 'above' the Zn-ion, orienting the carbonyl oxygen towards it and yielding ϕ/ψ angles of approximately 125°/145°. From this point towards the P-region, no orientation of the backbone for the substrate can be deduced from existing knowledge of the transition state analogue binding and natural inhibition. However, on the P-region there is evidence of specific sidechain interactions in the MMP-3/TIMP-1 complex [21], and a backbone H-bond (Figure 1): Ala167 from MMP-3 establishes a H-bond with Ser68 from the TIMP-1 inhibitor while His211 makes a H-bond with Glu67, which is also involved in hydrophobic interactions with Phe210 from

TIMP-1. Closer investigation of possible backbone torsions for the substrate shows that the next two residues on the substrate (P2 and P3) can satisfy the empirical criteria by adopting a β-sheet conformation (Figure 1). The four experimental residues were therefore added in a manner compatible with the existing β-sheet, which provided favorable H-bonded interactions between the P2 backbone atoms and Ala167 (Figure 1) as well as hydrophobic attraction between Phe210 and the P3-residue (Figure 1). This orientation was the only possibility that satisfied two requirements: (a) the orientation and position of the modeled scissile bond are in accord with both the reported synthetic transition state analogue and the natural inhibitor [21, 23]; and (b) the substrate should be in an extended beta-sheet conformation between the P2-P2′ residues for proteolysis to occur [41, 42].

At this stage, the addition of complementary residues was carried out in accord with empirical results (see Methods). In summary, we have built a model of the MMP3/substrate complex that satisfies all known experimental constraints. This enzyme–substrate complex was then used to build the equivalent enzyme–substrate models for ADAM-9 and ADAM-10.

Refinement and molecular simulation

MMP-3 and substrate

The MMP-3–substrate complex was stable throughout the simulation: the Cα-RMSD between the enzyme at start and end of simulation was 0.18 nm (Figure 3) and the rigid secondary structure elements were conserved well (Figure 4). The substrate remained in its original β-sheet conformation between P1-P3′ (Figure 5A). The backbone H-bonds of the P-region on the substrate of MMP-3 were slightly flexible at the end (P3 and P4); however, P2 and Ala167 remained H-bonded throughout the simulation.

Sidechain interactions were monitored using contact maps combined with visual inspection (Figures 5 and 7) and show that the S1′-cavity remained confined by Leu164, Val198 and Pro221, as originally reported by Dhanaraj et al. [14, 15]. The other interactions on the P′-region are listed in Table 2.

The hypothetical P-region showed interesting results. The P1-sidechain (Ala) had alternative orientations of its methyl group towards the solvent, His166 and between Pro221 and His211. Given these many alternatives in orientations of the P1-sidechain, and the weak chemical variability among the MMPs in this region [43] it is possible that no specific S1-position, or 'pocket' occurs in these enzymes, something that could be explained by the presence of the zinc ion, which requires a particular electrostatic environment for activity. Moving down the sequence, the P2 residue found a hydrophobic pocket defined mainly by Ala169 and the hydrophobic moiety of Ser206, while the P3 residue interacts mainly with Phe210. All of these residues are involved in the binding of TIMP-1 [21]. P4 interacts with Phe210 to some extent but mostly with Phe86, which extends from the N-terminal coil. This can be seen by the dark region of the contact maps (Figure 7) at the first 12 residues of the simulations of MMP-3 with substrate. The N-terminus was shown previously to be involved in binding TIMP-1 [21] and to be induced towards the binding cleft by peptidomimetics [23]. It seems therefore that the substrate as modelled here yields plausible interactions after homology modeling and molecular dynamics.

In summary, for the MMP-3 crystal structure (with 5 added residues), the observed orientation of the sidechains from the P-region indicates that there is a large hydrophobic valley, which interacts with the P2/P3 groups. Residues Ala169, Ser206 and Phe210 define this S2/S3 valley. As we shall see, this region is different in ADAM-9 and ADAM-10, but nevertheless it hosts the P2/P3 residues of their respective substrates in a similar manner.

ADAM-9 and substrate. In the two simulations of ADAM-9 in complex with its substrate the Cα RMSD from the starting structure were quite similar (Figure 3); however, they deviated more (roughly 0.1 nm) from the starting structure than the corresponding simulation of MMP-3 with substrate. The higher RMSD compared to the crystal structure is mainly caused by a flexibility of the region near the Met-turn and the parallel β-anchor, while the α-helices and the five β-strands (including the substrate-binding β-strand) were well preserved throughout the simulations (Figure 4). The H-bonding network between the substrate and the enzyme remained intact in the simulations as well. The P4 backbone atoms established a 'new' H-bond with the backbone atom of Val318, while the P2′ residue exchanged a backbone H-bond with the parallel β-anchor for a H-bond with the sidechain of Asn373 from the same anchor, indicating that the substrate is somewhat flexible. The remaining residues maintained the original H-bonding pattern, indicating that the complex was well preserved structurally,

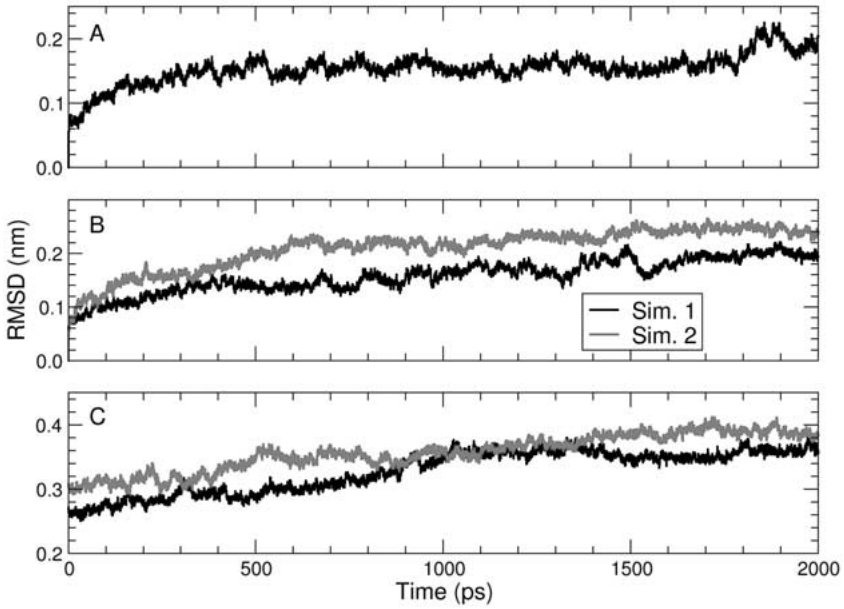

Figure 3. C-α root mean square deviation (RMSD) of the three complexes with respect to the starting structures for (A) MMP-3, (B) ADAM-9, and (C) ADAM-10.

and that its sidechains could be analyzed for subsite interactions.

The subsite interactions at the S1′ pocket in ADAM-9 were defined by Ala313, Ile344 and Asn373 (equivalent Leu164, Val198 and Pro221 in MMP-3, Figure 5B). The main specificity determinants here are Ala313 and Ile344 and given the hydrophobic identity of the P1′ sidechain (Val), the interactions were favorable. One polar residue, Ser343, occurs in this pocket, which seems to orient its sidechain into the enzyme. This residue does not correspond to the main determinants noted for MMP-3 by Dhanaraj et al. [14, 15], although it could still play a role in selectivity.

The S1 position in ADAM-9 (Met315) is analogous to MMP-3, where S1 is represented by the sidechain of residue His166 (MMP numbering). Some interactions with the solvent were found as well. However, at the end of both simulations the sidechain of tyrosine (at P1) was gently inclined towards Met315, suggesting that the P1-sidechain is flexible as it was in the MMP3-complex reference run. No indication of specific P1-S1 interaction could be found.

The new S2/S3 pocket in ADAM-9 is quite distinct from that of MMP-3. Val318, Asn352 and Asn356 constitute this region in ADAM-9 compared to Ala169, Ser206 and Phe210 in MMP-3. The trend of the P2/P3 residues orienting their sidechains in this wide but shallow cavity occurred in both simulations, analogous to the MMP3 simulation (Figure 5B).

ADAM-10 and substrate. The two simulations of ADAM-10 produced final conformations with a relatively high RMSD with respect to the start conformation (0.34 nm and 0.31 nm, respectively, averaged over the last 1000 ps of the simulations, see Figure 3). This mainly reflects a closure of the long reprolysin loop, which originally was modelled without a homologue template segment (Figure 6). The secondary structure of ADAM-10 is maintained throughout the simulations (Figure 4). The substrate of ADAM-10 remained more firmly bound on the P′-region than the P-region, as also observed in the reference simulation of MMP-3 with substrate, but experienced a loss of one of the initial H-bonds on the P-region (between P2 and backbone of Ala330). The reason for this was that the P2 (Gly) residue, due to its inherent flexibility, allowed for an inverse β-turn conformation. This may be induced by electrostatic attraction from the Zn-ion to the backbone oxygens from the central P-residues (P1 and P2), yielding both carbonyl oxygens in coordination with it. However, this could be an artefact, considering the precise Zn-ligation data that is available [44].

The primary specificity pocket S1′ is mainly determined by the sidechains of Leu327, Thr379 and Ala418, of which Thr379 pointed its hydroxyl group

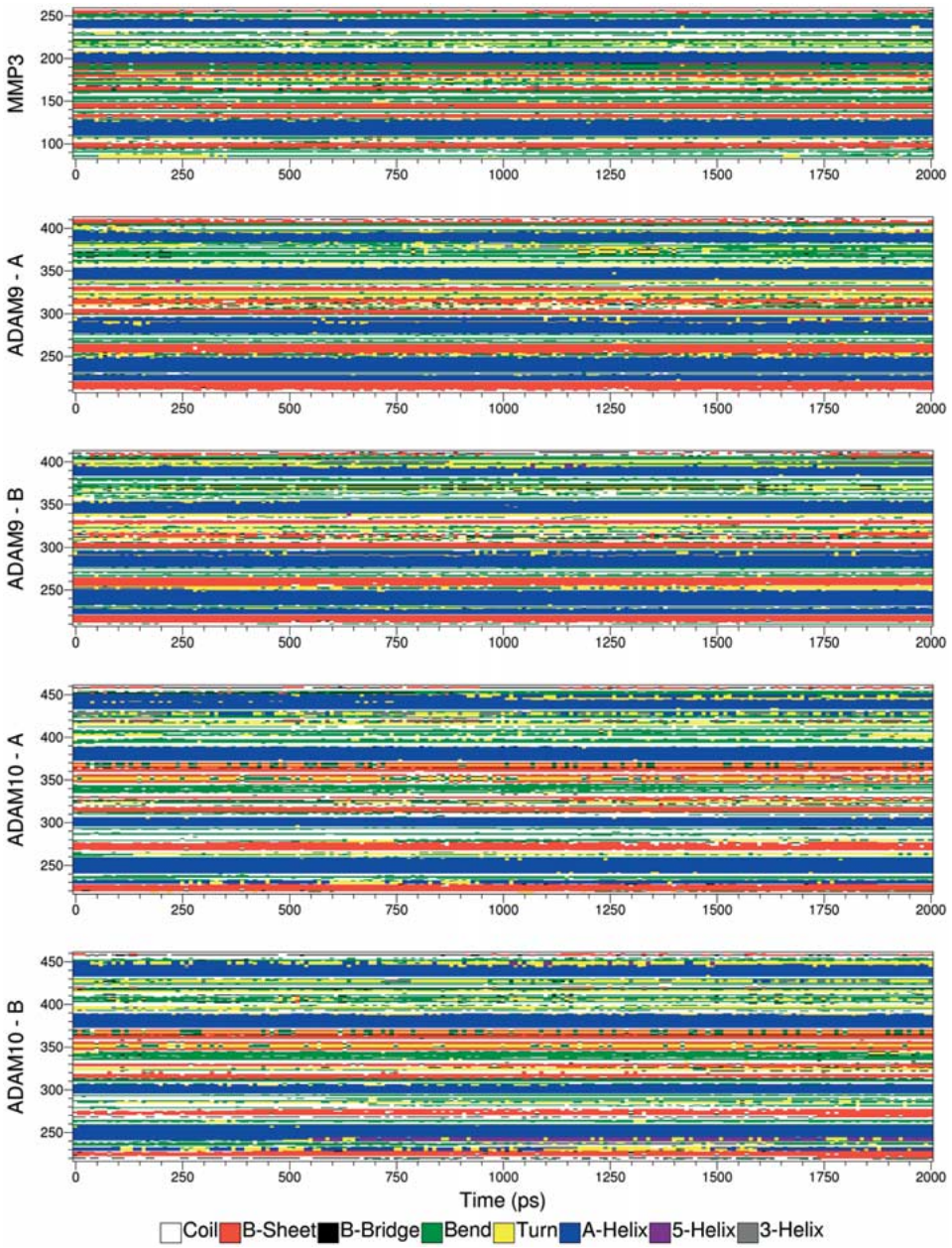

Figure 4. Secondary structure for each residue (on Y-axis) as a function of time (X-axis) using color codes to identify the different secondary structure types [56], for each of (from top to bottom) MMP3, ADAM-9 (Sims. 1 and 2) and ADAM-10 (Sims. 1 and 2). Secondary structure determined using the DSSP program [57]. Note that the main structure types (α-helix and β-sheet) are well preserved in all simulations.

away from the hydrophobic P1′ residue (Val, Figure 5C). The main determinants Thr379 and Leu327 (compared to MMP-3 subsites) indicate therefore a putative amphiphilic preference as the primary specificity of ADAM-10.

The S1-position is represented by Leu329, which is located on the opposite side of the substrate as where the Zn-ion is, equivalent to His166 in the MMP-3/substrate complex, and Met315 in ADAM-9. Here too, an interaction between solvent and sidechain was observed, showing that this position does not maintain specific interactions.

Because of the inverse β-sheet torsion of the glycine at the P2 position, unexpected interactions took

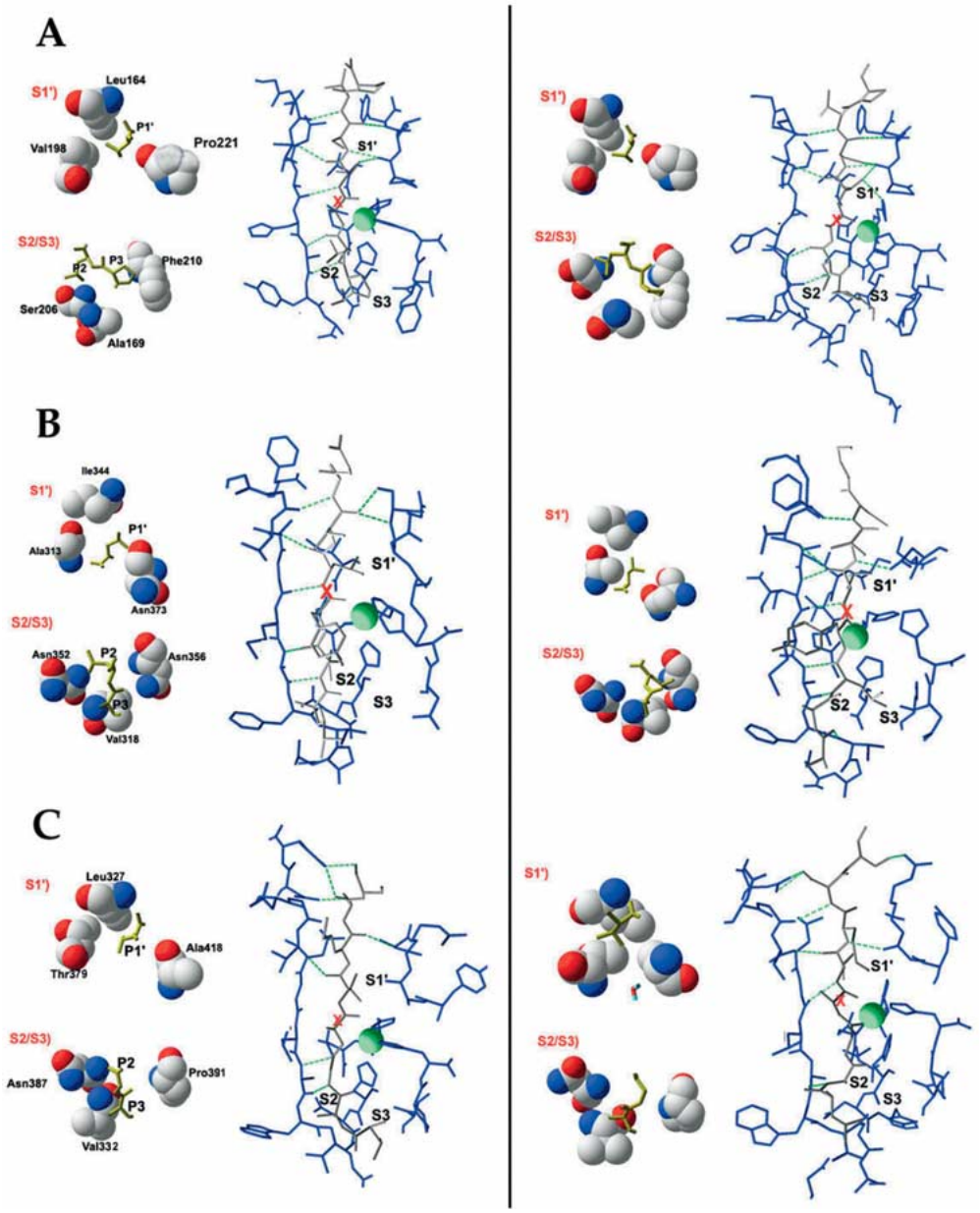

Figure 5. Structural changes at the binding pockets of (A) MMP-3, (B) ADAM-9 (Sim. 1), and (C) ADAM-10 (Sim. 1). Left: before simulation, right: after simulation. The two columns show the binding pockets with the H-bond network in green, and the substrate recognizing subsites, denoted with S1′ and S2/S3. A water molecule is found in the lower left S1′ subsite, shown in stick mode.

place as the P3-residue reoriented and established a H-bond with the carbonyl oxygen from Ala330 (which was originally H-bonded to P2). As a consequence, Val332 dominated the attraction to the P3-residue in both simulations. However, the S2/S3 valley is formed here by Val332, Asn387 and Pro391 (Figure 5).

The structural differences between the enzymes indicate that there are differences in primary specificity between them as well. These differences are similar to those found in e.g. elastases and chymotrypsins from the serine protease family, which cleave small hydrophobic proteins and bulky ones with a polar tip [45], generating complementary hydrolysis patterns in extracellular and intracellular functioning. ADAM-9 and MMP-3 share hydrophobic preferences at the S1′-position, while ADAM-10 can be anticipated to

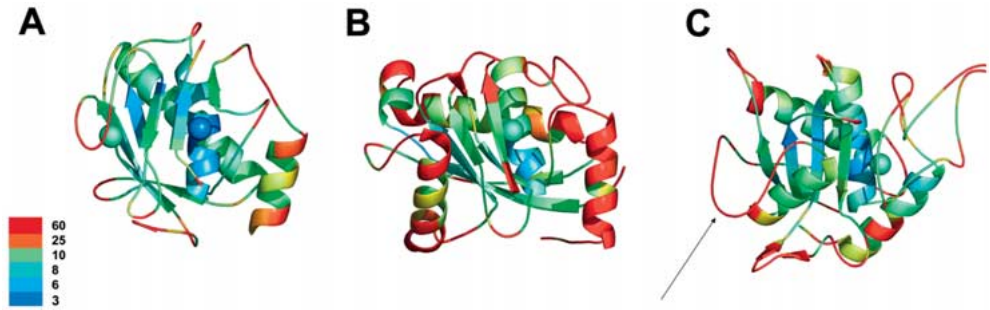

Figure 6. Simulated B-factors (unit 0.01 nm^2) from the second ns of the trajectories for (A) MMP-3, (B) ADAM-9 (Sim. 1), and (C) ADAM-10 (Sim. 1). The positional mean square fluctuations were computed and multiplied by $8*\pi/3$ to obtain B-factors. The arrow in C points to the reprolysin loop. Calcium ions from MMP-3 are not shown for the purpose of clarity.

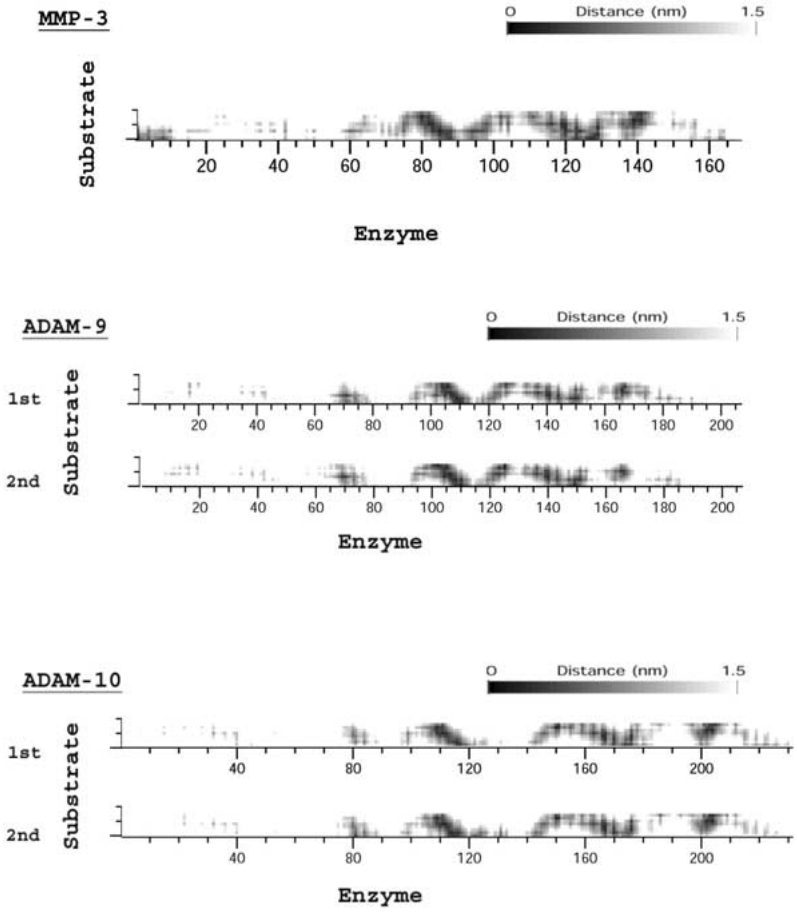

Figure 7. Contact maps for enzyme–substrate interactions. Distance interaction matrix computed over the last ns of the simulations for each complex. The two matrices for each complex illustrate the short distances (dark spots) and longer distances (lighter spots) between the interacting residues on the enzyme (horizontal) and on the substrate (vertical). The most important interactions (shortest distances) are listed in Table 2.

prefer small amphiphilic residues, such as serine or threonine. At the S2/S3 pocket, typical hydrophobic preferences are predicted for all three enzymes, based on the subsite information from Table 2. In preliminary simulations with negatively charged residues the coordination of the Zn-ion was disturbed (data not shown), which interferes with the requirement of an optimal electronic environment for activity [44]. We therefore conclude that all three enzymes prefer neutral residues at the S1-positions.

The catalytic center – a hypothetical catalytic mechanism

During all five MD simulations the catalytic Zn^{2+} attracted the side chain of the catalytic glutamate (from the zinc-binding motif). In four of five simulations, no water molecule went in coordination with the zinc ion (the fifth simulation, ADAM-9 run 2, experienced a disruption of the Met-turn). We realize that such observations must be interpreted with utmost care because it is problematic to model metal ions realistically without explicit polarization and/or charge transfer. Hence, the formal charge of +2 that was used for the Zn-ion, although correct from a large distance, may lead to local artifacts, like, perhaps, the rearrangement of the Gly backbone in the ADAM-10 simulation. Furthermore, the restraints on the Zn-ion could in principle limit its mobility although the restraint forces are weak (see Methods). Nevertheless, the glutamate movement that we noted in the simulations has been observed previously in MMP-3 and carboxypeptidase A [21, 46]. Parkin [47] reported that the Zn^{2+}-ion in MMPs is likely to be tetra-coordinated with the His-triad and a water molecule, in the ground state, which is in accord with the results supplied by Alberts et al. [44]. However, some structures of MMP-holoenzymes show that the catalytic Zn^{2+}-ion is tri-coordinated with the three His-residues, even in the presence of adjacent water molecules [23, 48]. Interestingly, Gall et al. [43] reported that the catalytic zinc in MMP-11 is tetra-coordinated when complexed with an inhibitor, mimicking the transition state, and no water molecule is in coordination with the Zn-ion. This trend was also observed by other groups who crystallized various metzincins in complex with transition state analogues [14, 15, 48–50]. This represents at least six distinct observations providing strong evidence that water is not bound to the Zn-ion during a transition state for these enzymes. Additionally, in these very structures, the side-chain oxygens of the catalytic glutamic acid are observed in various coordinations with the zinc, some with both oxygens, others with one.

Inspired by the movement of the catalytic Glu towards the Zn-ion in the simulations and the experimental observations mentioned above, we propose a novel, hypothetical, catalytic mechanism. We suggest that the Zn-ion is penta-coordinated in the transition state, primarily because of the large amount of structural evidence where no water is present [14, 15, 21, 48–51], but also because a Zn–water interaction was not observed in our simulations. The five coordinators of the Zn-ion in the transition state are proposed to be the two ε-nitrogens from the histidines on the short spacer, the P1′-carbonyl and the two oxygen atoms from the catalytic glutamate (based on the putative flexibility of the third histidine from the long spacer [47]). This set of empirical and computational results and observations leads us to suggest a new catalytic mechanism for the metzincins, based on the formation of an anhydride intermediate (as was observed for carboxypeptidases [44]). This mechanism supports (a) the various inclinations observed between the two oxygens from the catalytic glutamate and the catalytic Zn-ion [14, 15, 21, 48, 51], (b) the various crystal structures of transition state analogues with expelled water molecules [14, 15, 21, 48, 51] and (c) the observed flexibility of the catalytic glutamate to approach the Zn-ion in our simulations as well as empirically [21], and (d) the hypothesized flexibility of the third histidine [45].

In this mechanism (Figure 8), the catalytic glutamate moves in coordination with the Zn-ion where the glutamate Oε is polarized, leading to the formation of a nucleophilic oxygen atom, similar to the catalytic Ser195 in the serine-protease catalytic mechanism [52] (state 1). The carbon atom from the scissile bond, which is polarized through its carbonyl oxygen by the Zn^{2+}-ion, becomes a weak carbo-cation, and accepts an electron from the polarized nucleophilic Oε of the catalytic glutamate. This forms a transient bond between the enzyme and the substrate creating an oxyanion-tetrahedral anhydride intermediate (state 2), a formation investigated for carboxypeptidase A [44, 53]. The oxyanion transition state, which is unstable, induces the electron towards the amide nitrogen, breaking the scissile bond (state 3). The short-lived anhydride bond (between the enzyme and the substrate) is believed to induce a polarization effect from the Zn-ion on the second ε-oxygen, which facilitates the electron transfer from the carbonyl carbon back to the glutamate's first ε-oxygen, breaking the co-

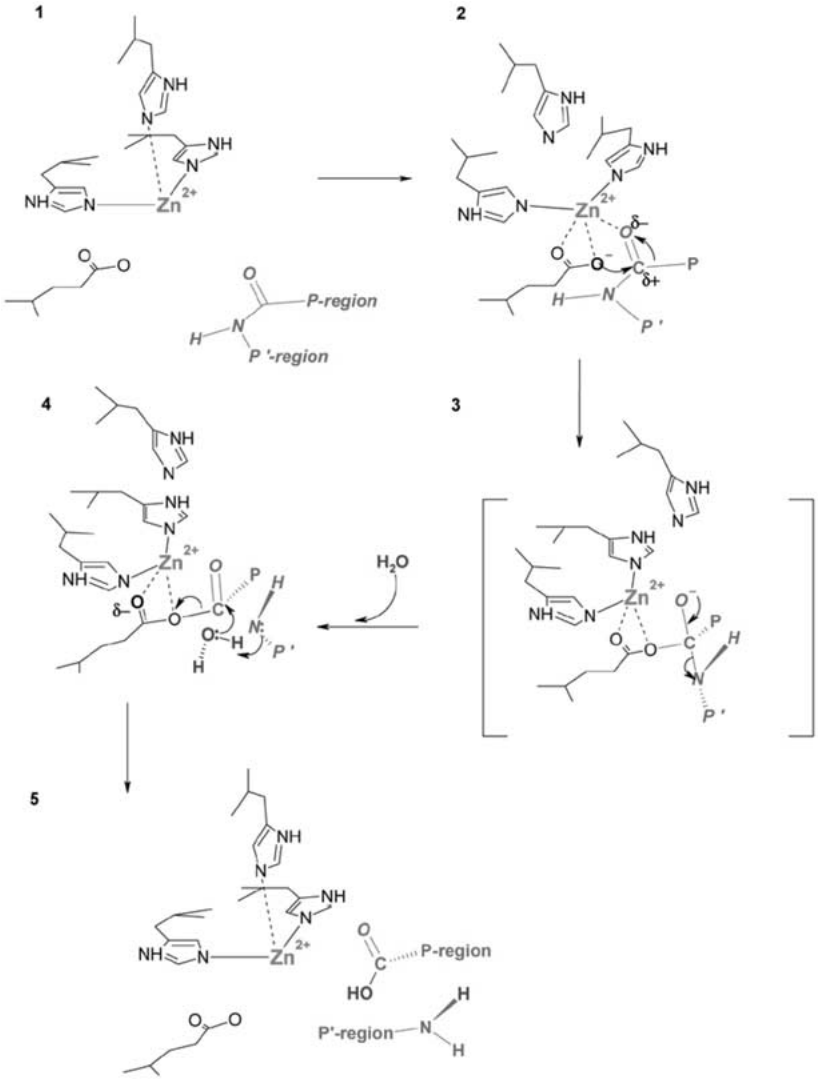

Figure 8. A hypothetical catalytic mechanism for the metzincin superfamily. *State 1*: The Zn-ion is in its tri-coordinated resting state. *State 2*: The third histidine moves out of coordination from the Zn-ion [47], and the quasipenta-coordinated Zn-ion influences the Oε of the glutamate side chain to act as an aggressive base, which transfers an electron to the carbocation on the scissile bond (polarized by the Zn ion), creating an oxyanion transition state. *State 3*: The tetrahedral intermediate, the electron transfer leads the electron to the amide nitrogen given the high-energy state of the negatively charged oxygen, breaking the scissile bond. *State 4*: The anhydride bond breaks, given the inclination of the second glutamate oxygen to the Zn-ion, and a water molecule protonates the leaving group and hydroxylates the new C-terminus. *State 5*: The Zn-ion goes back in coordination with the third histidine, and the cleaved substrate detaches.

valent E-S state (state 4). In concert with this, a water molecule close to the amide bond acts as an acid upon the nitrogen atom, creating the leaving group. The formed hydroxyl group acts as a base on the carbonyl thereby yielding the new C-terminus.

With regard to the role of water during catalysis, as speculated by Browner et al. [12], our study shows that in order to fit a water molecule between the substrate and the Zn^{2+}-ion at an optimal angle for both successful polarization (through orientation and proximity effects [54]) and maintenance of the crucial H-bonds between backbone atoms of the enzyme and the P′-region [29], an expansion of the binding pocket from 0.66 nm to more than 1.1 nm would be required. This is a movement comparable to that seen in allosteric enzymes [55] and, according to existing data [21, 23], MMP-3 only moves its N-terminal residues towards the P-region of the substrate upon binding. Our

enzyme–substrate complex indicates, therefore, that a mechanism without water, possibly the one suggested here, would be more logical.

Conclusions

We have built models of MMP-3, ADAM-9 and ADAM-10 in complex with *in vitro* based substrates, and refined them using molecular dynamics simulations in explicit solvent. The enzyme–substrate complex of MMP-3 proved to be stable during the molecular dynamics simulation (Figures 3 and 4), whereas the models of ADAM-9 and ADAM-10, that were built on a rather low homology (30 and 31%, respectively), showed a satisfactory stability of the core in the molecular dynamics experiments and a stable secondary structure as well (Figure 3). It seems, therefore, that the resulting models are plausible and we think that the complexes deduced in this work, with all the substrate binding particulars that we have analyzed, will be particularly useful for predicting substrates for assays.

Inspired by the movement of the catalytic glutamate and with support from the literature, we have proposed a novel catalytic mechanism (Figure 8) where the catalytic glutamate acts as a nucleophile, fixed by the Zn-ion which simultaneously polarizes the scissile carboxyl group.

Atomic coordinates

ADAM-9, ADAM-10 and MMP-3 in complex with their substrates, before and after simulation, have been deposited in the protein databank as 1KNH, 1M1I and 1KN8 entries, respectively.

Acknowledgments

The authors would like to thank Prof. Torsten Schwede for constructive criticism of modeling approaches, Prof. Arieh Warshel, Dr Terry Walsh and Mr Trygve Stensrud for critical discussion on the mechanism. We would also like to thank Prof. Ross Barnard for discussion on the Zn-chelating state and the High Performance Computing Group from Queensland University of Technology for providing access to appropriate computing hardware.

References

1. Basbaum, C.B. and Werb, Z., Curr. Opin. Cell. Biol. 8 (1996) 731.
2. Nagase, H., Matrix metalloproteinase. In: Hooper, N. (ed.), Zinc Metalloproteinases in Health and Disease. Taylor and Francis, London, 1996, pp. 153–204.
3. Primakoff, P. and Myles, D.G., Trends Genet., 16 (2000) 83.
4. Millichip, M.I., Dallas, D.J., Wu, E., Dale, S. and McKie, N., Biochem. Biophys. Res. Commun., 245 (1998) 594.
5. Vincent, B., Paitel, E., Saftig, P., Frobert, Y., Hartmann, D., De Strooper, B., Grassi, J., Lopez-Perez, E. and Checler, F., J. Biol. Chem., 276 (2001) 37743.
6. Kiyama, R., Tamura, Y., Watanabe, F., Tsuzuki, H., Ohtani, M. and Yodo, M., J. Med. Chem., 42 (1999) 1723.
7. Rosendahl, M.S., Ko, S.C., Long, D.L., Brewer, M.T., Rosenzweig, B., Hedl, E., Anderson, L., Pyle, S.M., Moreland, J., Meyers, M.A., Kohno, T., Lyons, D. and Lichenstein, H.S., J. Biol. Chem., 272 (1997) 24588.
8. Roghani, M., Becherer, J.D., Moss, M.L., Atherton, R.E., Erdjument-Bromage, H., Arribas, J., Blackburn, R.K., Weskamp, G., Tempst, P. and Blobel, C.P., J. Biol. Chem., 274 (1999) 3531.
9. Springman, E.B., Angleton, E.L., Birkedal-Hansen, H. and Van Wart, H.E., Proc. Natl. Acad. Sci. USA, 87 (1990) 364.
10. Stocker, W., Grams, F., Baumann, U., Reinemer, P., Gomis-Rüth, F.X., McKay, D.B. and Bode, W., Protein Sci., 4 (1995) 823.
11. Reinemer, P., Grams, F., Huber, R., Kleine, T., Schnierer, S., Piper, M., Tschesche, H. and Bode, W., FEBS Lett., 338 (1994) 227.
12. Browner, M.F., Smith, W. and Castelhano, A.L., Biochemistry, 34 (1995) 6602.
13. Lovejoy, B., Cleasby, A., Hassell, A.M., Longley, K., Luther, M.A., Weigl, D., McGeehan, G., McElroy, A.B., Drewry, D., Lambert, M.H. and Jordan, S.R., Science, 263 (1994) 375.
14. Dhanaraj, V., Ye, Q.Z., Johnson, L.L., Hupe, D.J., Ortwine, D.F., Dunbar, J.B., Rubin, J.R., Pavlovsky, A., Humblet, C. and Blundell, T.L., Structure, 4 (1996a) 375.
15. Dhanaraj, V., Ye, Q.Z., Johnson, L.L., Hupe, D.J., Ortwine, D.F., Dunbar, J.B. Jr., Rubin, J.R., Pavlovsky, A., Humblet, C. and Blundell, T. L., Drug. Des. Discov., 13 (1996b) 3.
16. Murphy, G. and Docherty, J.P., Am. J. Res. Cell. Mol. Biol., 7 (1992) 120.
17. Amour, A., Slocombe, P.M., Webster, A., Butler, M., Knight, C.G., Smith, B.J., Stephens, P.E., Shelley, C., Hutton, M., Knauper, V., Docherty, A.J. and Murphy, G., FEBS Lett., 435 (1998) 39.
18. Amour, A., Knight, C.G., Webster, A., Slocombe, P.M., Stephens, P.E., Knauper, V., Docherty, A.J. and Murphy, G., FEBS Lett., 473 (2000) 275.
19. Heath, E.I. and Grochow, L.B., Drugs, 59 (2000) 1043.
20. Guex, N. and Peitsch, M.C., Electrophoresis, 18 (1997) 2714.
21. Gomis-Rüth, F.X., Maskos, K., Betz, M., Bergner, A., Huber, R., Suzuki, K., Yoshida, N., Nagase, H., Brew, K., Bourenkov, G.P., Bartunik, H. and Bode, W., Nature, 389 (1997) 77.
22. Berman, H.M., Westbrook, J., Feng, Z., Gilliland, G., Bhat, T.N., Weissig, H., Shindyalov, I.N. and Bourne, P.E., Nucleic Acids Res., 28 (2000) 235.
23. Chen, L., Rydel, T.J., Dunaway, C.M., Pikul, S., Dunham, K.M., Gu, F. and Barnett, B.L., J. Mol. Biol., 293 (1999) 545.
24. Smith, M.M., Shi, L. and Navre, M., J. Biol. Chem., 270 (1995) 6440.

25. Weskamp, G., Kratzschmar, J., Reid, M.S. and Blobel, C.P., J. Cell. Biol., 132 (1996) 717.
26. Karplus, K., Barrett, C. and Hughey, R., Bioinformatics, 14 (1998) 846.
27. Johnson, L.L., Pavlovsky, A.G., Johnson, A.R., Janowicz, J.A., Man, C.F., Ortwine, D.F., Purchase II, C.F., White, A.D. and Hupe, D.J., J. Biol. Chem., 275 (2000) 11026.
28. Scott, W.R.P., Hünenberger, H.P., Tironi, I.G., Mark, A.E., Billeter, S.R., Fennen, J., Torda, A.E., Huber, T., Krüger, P. and Van Gunsteren, W.F., J. Phys. Chem., B 103 (1999) 3596.
29. Berendsen, H.J.C., Postma, J.P.M., Van Gunsteren, W.F. and Hermans, J. In Pulman, B. (Ed.) Intermolecular Forces. D. Reidel Publishing Company, Dordrecht, 1981, pp. 331–342.
30. Lindahl, E., Hess, B. and Van der Spoel, D., J. Mol. Mod., 7 (2001) 306.
31. Hess, B., Bekker, H., Berendsen, H.J.C. and Fraaije, J.G.E.M., J. Comput. Chem., 18 (1997) 1463.
32. Miyamoto, S. and Kollman, P.A., J. Comput. Chem., 13 (1992) 952.
33. Jones, S.T., Ahlström, P., Berendsen, H.J.C. and Pickersgill, R.W., Biochim. Biophys. Acta, 1162 (1993) 135.
34. Berendsen, H.J.C., Postma, J.P.M., DiNola, A. and Haak, J.R., J. Chem. Phys., 81 (1984) 3684.
35. Darden, T.A., York, D.M. and Pedersen, L.G., J. Chem. Phys., 98 (1993) 10089.
36. Feierberg, I., Cameron, A.D. and Åqvist, J., FEBS Lett., 453 (1999) 90.
37. Gomis-Rüth, F.X., Kress, L.F. and Bode, W., EMBO J., 12 (1993) 4151.
38. Zhang, D., Botos, I., Gomis-Ruth, F.X., Doll, R., Blood, C., Njoroge, F.G., Fox, J.W., Bode, W. and Meyer, E.F., Proc. Natl. Acad. Sci. USA, 91 (1994) 8447.
39. Zhu, X., Teng, M. and Niu, L., Acta Cryst., D 55 (1999) 1834.
40. Maskos, K., Fernandez-Catalan, C., Huber, R., Bourenkov, G.P., Bartunik, H., Ellestad, G.A., Reddy, P., Wolfson, M.F., Rauch, C.T., Castner, B.J., Davis, R., Clarke, H.R., Petersen, M., Fitzner, J.N., Cerretti, D.P., March, C.J., Paxton, R.J., Black, R.A. and Bode, W., Proc. Natl. Acad. Sci. USA, 95 (1998) 3408.
41. Tyndall, J.D. and Fairlie, D.P., Curr. Med. Chem., 8 (2001) 893.
42. Glenn, M.P., Pattenden, L.K., Reid, R.C., Tyssen, D.P., Tyndall, J.D., Birch, C.J. and Fairlie, D.P., J. Med. Chem., 45 (2001) 371.
43. Gall, A.L., Ruff, M., Kannan, R., Cuniasse, P., Yiotakis, A., Dive, V., Rio, M.C., Basset, P. and Moras, D., J. Mol. Biol., 307 (2001) 577.
44. Alberts, I.L., Nadassy, K. and Wodak, S.J., Protein Sci., 7 (1998) 1700.
45. Perona, J.J. and Craik, C.S., Protein Sci., 4 (1995) 337.
46. Mustafi, D. and Makinen, M.W., J. Biol. Chem., 269 (1994) 4587.
47. Parkin, G., Met. Ions Biol. Syst., 38 (2001) 411.
48. Dhanaraj, V., Williams, M.G., Ye, Q.-Z., Molina, F., Johnson, L.L., Ortwine, D.F., Pavlovsky, A., Rubin, J.R., Skeean, R.W., White, A.D., Humblet, C., Hupe, D. and Blundell, T.L., Croatica Chem. Acta, 72 (1999) 575.
49. Seltzer, J.L., Weingarten, H., Akers, K.T., Eschbach, M.L., Grant, G.A. and Eisen, A.Z., J. Biol. Chem., 264 (1989) 19583.
50. Pavlovsky, A.G., Williams, M.G., Ye, Q.-Z., Ortwine, D.F., Purchase II, C.F., White, A.D., Dhanaraj, V., Roth, B.D., Johnson, L.L., Hupe, D., Humblet, C. and Blundell, T.L., Protein Sci., 7 (1999) 1455.
51. Borkakoti, N., Winkler, F.K., Williams, D.H., D'Arcy, A., Broadhurst, M.J., Brown, P.A., Johnson, W.H. and Murray, E.J., Nat. Struct. Biol., 1 (1994) 106.
52. Fersht, A., Enzyme Structure and Mechanism. W.H. Freeman and Company Ltd., San Francisco, USA, 1977, p. 27.
53. Mock, L., Zinc Proteinases. Comprehensive Biological Catalysis. Academic Press, USA, 1998. 431 pp.
54. Koshland, D.E. Jr., Carraway, K.W., Dafforn, G.A., Gass, J.D. and Storm, D.R., Cold Spring Harbor Symp. Quant. Biol., 36 (1972) 13.
55. Chothia, C., Wodak, S. and Janin, J., Proc. Natl. Acad. Sci. USA, 73 (1976) 3793.
56. Van der Spoel, D., Vogel, H.J. and Berendsen, H.J.C., Protein. Struct. Funct. Genet., 24 (1996) 450.
57. Kabsch, W. and Sander, C., Biopolymers, 22 (1983) 2577.